Ligand-Induced Structural Changes in Adenosine 5‘-Phosphosulfate Kinase from Penicillium chrysogenum † , ‡

ARTICLE *in* BIOCHEMISTRY · DECEMBER 2002

Impact Factor: 3.02 · DOI: 10.1021/bi026556b · Source: PubMed

3 AUTHORS, INCLUDING:

Eric B Lansdon
Gilead Sciences
24 PUBLICATIONS **514** CITATIONS
SEE PROFILE

Andrew Fisher
University of California, Davis
77 PUBLICATIONS **2,566** CITATIONS
SEE PROFILE

Ligand-Induced Structural Changes in Adenosine 5′-Phosphosulfate Kinase from *Penicillium chrysogenum*[†,‡]

Eric B. Lansdon,[§] Irwin H. Segel,[⊥] and Andrew J. Fisher*[,§,⊥]

Department of Chemistry and Section of Molecular and Cellular Biology, University of California, One Shields Avenue, Davis, California 95616

Received August 1, 2002; Revised Manuscript Received September 11, 2002

ABSTRACT: Adenosine 5′-phosphosulfate (APS) kinase catalyzes the second reaction in the two-step, ATP-dependent conversion of inorganic sulfate to 3′-phosphoadenosine 5′-phosphosulfate (PAPS). PAPS serves as the sulfuryl donor for the biosynthesis of all sulfate esters and also as a precursor of reduced sulfur biomolecules in many organisms. Previously, we determined the crystal structure of ligand-free APS kinase from the filamentous fungus, *Penicillium chrysogenum* [MacRae et al. (2000) *Biochemistry 39*, 1613−1621]. That structure contained a protease-susceptible disordered region ("mobile lid"; residues 145−170). Addition of MgADP and APS, which together promote the formation of a nonproductive "dead-end" ternary complex, protected the lid from trypsin. This report presents the 1.43 Å resolution crystal structure of APS kinase with both ADP and APS bound at the active site and the 2.0 Å resolution structure of the enzyme with ADP alone bound. The mobile lid is ordered in both complexes and is shown to provide part of the binding site for APS. That site is formed primarily by the highly conserved Arg 66, Arg 80, and Phe 75 from the protein core and Phe 165 from the mobile lid. The two Phe residues straddle the adenine ring of bound APS. Arg 148, a completely conserved residue, is the only residue in the mobile lid that interacts directly with bound ADP. Ser 34, located in the apex of the P-loop, hydrogen-bonds to the 3′-OH of APS, the phosphoryl transfer target. The structure of the binary E·ADP complex revealed further changes in the active site and N-terminal helix that occur upon the binding/release of (P)APS.

Inorganic sulfate is converted into a biologically "activated" form, 3′-phosphoadenosine 5′-phosphosulfate (PAPS),[1] via a two-step sequence catalyzed, in order, by the enzymes ATP sulfurylase (MgATP, sulfate adenylyltransferase, EC 2.7.7.4) and APS kinase (MgATP, APS 3′-phosphotransferase, EC 2.7.1.25):

$$MgATP + SO_4^{2-} \rightleftharpoons MgPP_i + APS \quad \text{(ATP sulfurylase)}$$

$$MgATP + APS \rightleftharpoons PAPS + MgADP \quad \text{(APS kinase)}$$

The sequences of APS kinases from over 30 different organisms show that this enzyme is highly conserved. In lower organisms, APS kinase exists as an independent enzyme, and the PAPS it produces is generally used for reductive sulfate assimilation (i.e., for the biosynthesis of cysteine, etc.). In mammals, the enzyme exists as part of a bifunctional "PAPS synthetase" that possesses both ATP sulfurylase and APS kinase activities (*1*−*3*). Mammals use PAPS solely for the production of sulfate esters, which play important roles in cellular homeostasis (*4*). The absence of one human isoform of PAPS synthetase has been associated with metastatic cell behavior in colon carcinoma cells (*5*). Most kinetics studies of APS kinase have focused on the enzymes from *Penicillium chrysogenum* (*6*−*8*), *Escherichia coli* (*9*−*11*), *Arabidopsis thaliana* (*12*, *13*) and rat chondrosarcoma cells (*14*, *15*).

APS kinase from the filamentous fungus *P. chrysogenum* is a homodimer, each 23.67 kDa monomer subunit containing 211 amino acid residues. Steady-state kinetics have shown that the enzyme follows a compulsory ordered mechanism in which MgATP binds before APS, and PAPS leaves before MgADP (*6*). APS can bind to E·MgADP, forming a catalytically inactive ("dead-end") ternary E·MgADP·APS complex. The formation of this complex is the basis of the substrate inhibition exhibited by APS (*6*, *16*). Substrate inhibition has also been reported for other APS kinases, including the closely related (sequence-wise) *E. coli* enzyme (*9*−*11*), but the kinetic mechanism of the bacterial enzyme

[†] This work was supported in part by NSF Grant MCB-9904003 to I.H.S. and A.J.F. and the W. M. Keck Foundation Center for Structural Biology at the University of California, Davis. E.B.L. is supported by the University of California System-wide Biotechnology Research Program Grant No. 2001-07. All the data presented in this report were collected at SSRL, which is operated by the Department of Energy, Office of Basic Energy Sciences. The SSRL Biotechnology Program is supported by the National Institutes of Health, National Center for Research Resources, Biomedical Technology Program, and by the U.S. Department of Energy, Office of Biological and Environmental Research.

[‡] Protein coordinates have been deposited in the Protein Data Bank (IDs 1M7G and 1M7H for the ternary and binary complexes, respectively).

* Corresponding author. Phone: (530) 754-6180. Fax: (530) 752-8995. E-mail: fisher@chem.ucdavis.edu.

[§] Department of Chemistry.

[⊥] Section of Molecular and Cellular Biology.

[1] Abbreviations: APS, adenosine 5′-phosphosulfate (adenylyl sulfate); PAPS, 3′-phosphoadenosine 5′-phosphosulfate (adenylyl sulfate 3′-phosphate); MgATP and MgADP, magnesium complexes of adenosine 5′-triphosphate and adenosine 5′-diphosphate respectively; Tris, tris-hydroxymethylaminomethane; MAD, multiple wavelength anomalous dispersion; RMSD, root-mean-square deviation.

10.1021/bi026556b CCC: $22.00
Published on Web 10/25/2002

Table 1: Data Collection, Phasing, and Refinement Statistics

	Br^- peak	Br^- remote	Br^- inflection	native	APS free soak
X-ray source	BL 9-2	BL 9-2	BL 9-2	BL 9-1	BL 9-2
wavelength (Å)	0.9196	0.8610	0.9198	0.9700	0.9800
resolution (Å)	1.90	1.90	1.90	1.43	2.00
no. of reflections	509 621	456 897	458 508	3 135 818	621 412
no. unique reflections	75 497	75 881	74 990	174 517	64 678
R_{merge}[a] (%)	7.4 (39.7)	7.0 (36.4)	9.6 (51.9)	4.9 (39.9)	5.0 (32.9)
completeness (%)	99.3 (98.7)	99.3 (97.4)	98.0 (96.2)	99.3 (98.0)	97.3 (91.5)
no. of sites	13	13	13		
figure of merit		0.29			
		Refinement Statistics			
resolution (Å)				30−1.43	30−2.00
no. of reflections ($F \geq 0$)				174 517	64 678
R-factor[b]				18.0	21.5
R-free[b]				20.5	25.8
RMS bond length				0.015	0.009
RMS bond angle				1.7	1.4
		Asymmetric Unit Content			
non-hydrogen protein atoms				6177	6390
water				790	499
sulfates (no. of molecules)				30 (6)	60 (12)
vanadium				2	
glycerol (no. of molecules)				18 (3)	

[a] $R_{merge} = [\sum_h \sum_i |\boldsymbol{I}_h - \boldsymbol{I}_{hi}| / \sum_h \sum_i \boldsymbol{I}_{hi}]$, where $\boldsymbol{I}_h$ is the mean of $\boldsymbol{I}_{hi}$ observations of reflection h. Numbers in parentheses represent highest resolution shell. [b] R-factor and R-free $= \sum ||F_{obs}| - |F_{calc}|| / \sum |F_{obs}| \times 100$ for 95% of recorded data (R-factor) or 5% of data (R-free). Numbers in parentheses represent highest resolution shell.

may be different. The bacterial enzyme is believed to proceed via a phosphorylated enzyme intermediate. The phosphoryl acceptor has been identified as Ser 109, which is analogous to Ser 107 of the *P. chrysogenum* enzyme. However, in the fungal enzyme, Ser 107 is nonessential for activity (*17*).

APS kinase from *P. chrysogenum* (*18*) belongs to the purine nucleotide-binding superfamily of protein folds. It shows high structural homology to the bifunctional 6-phosphofructo-2-kinase/2,6-phosphofructo-2-phosphatase, despite sharing only 9% identity with that protein. As expected, APS kinase contains a Walker A motif (*19*), ^{32}GLSASGKS^{39}. This motif forms the P-loop, which provides the triphosphate binding site of nucleoside triphosphates. The structure of apo-APS kinase revealed a disordered region of amino acids (145−170) in both subunits of the dimer. This region was highly susceptible to trypsin cleavage at Arg 158 (*18*). MgADP plus APS protected against trypsin action, suggesting that this flexible region (termed the "mobile lid") is stabilized upon the binding of active site ligands.

This current study was pursued in order to answer several key questions: (a) What is the structural basis of the sequential ordered mechanism and of substrate inhibition? (b) Which residues are involved in substrate binding and catalysis? (c) Why is dimerization important for catalysis? To answer these questions, *P. chrysogenum* APS kinase was crystallized in the presence of ADP and APS and solved to 1.43 Å resolution. After APS was soaked out of the crystal, the structure of the resulting E·ADP binary complex was solved at 2.0 Å resolution. When compared to the structures of the apo enzyme and the E·ADP·APS complex, this E·ADP structure revealed the changes that occur upon the binding/release of (P)APS.

EXPERIMENTAL PROCEDURES

Protein Expression and Crystallization. The cDNA encoding wild-type APS kinase from *P. chrysogenum* had previously been cloned into a pET expression system (*17*). After APS kinase expression and purification (*16*), the enzyme was dialyzed against 10 mM Tris buffer, pH 8.0, and concentrated by membrane filtration to about 10 mg/mL. Prior to crystal setup, APS kinase was mixed with 3 mM MgADP and 3 mM APS. Crystals were grown in 1.7 M NaH_2PO_4, 0.3 M K_2HPO_4, and 0.1 M Na succinate, pH 4.0, by hanging-drop vapor diffusion at room temperature. Crystals typically appeared over the course of a week and continued to grow over three weeks. The crystals, which grew as flat plates up to 1.0 mm × 1.0 mm × 0.3 mm in size, belong to the orthorhombic space group $P2_12_12_1$ with unit cell dimensions $a = 81.5$ Å, $b = 84.5$ Å, and $c = 137.5$ Å. The Matthews V_M coefficient was 2.46 Å^3/Da, with a solvent content of 49.5%, assuming two copies of the dimer in the asymmetric unit. Crystals were introduced into a 20% glycerol cryoprotectant solution in a stepwise manner by increasing the glycerol concentration in three increments (from 7% to 14% to 20%). The crystals were transferred through the solution over the course of 1 min and cooled in a stream of nitrogen vapor at 100 K. These crystals typically diffracted X-rays to 2.50 Å on a rotating anode.

Transferring the crystals into a new mother liquor containing 1.7 M $(NH_4)_2SO_4$ and Bis-Tris Cl (pH 6.5) supplemented with ADP and APS extended the resolution to 2.00 Å on a rotating anode. The crystals were allowed to equilibrate in the new mother liquor for at least 24 h. The highest resolution was obtained with crystals that had equilibrated for up to one week.

Data Collection and Phase Determination. A 1.43 Å resolution native data set from a crystal soaked in ammonium sulfate was collected at Beamline (BL) 9-1 at SSRL (Table 1). Numerous molecular replacement attempts using the previously determined apo structure of APS kinase (both monomer and dimer) and different algorithms did not yield a solution. Fungal APS kinase contains no cysteine or

methionine. Thus, the chances of forming a heavy-atom derivative were greatly reduced. Seleno-methionine replacement was not possible because the N-terminal methionine had been processed off. After many attempts to derivatize with heavy atoms, a NaBr soak was attempted to introduce halide atoms for MAD phase determination (*20*, *21*). Through trial and error, it was determined that crystals soaked in 0.75 M NaBr for 45 s did not greatly reduce diffraction. Crystals were introduced to the glycerol cryoprotectant and NaBr at the same time in the stepwise manner described previously. The crystal was allowed to equilibrate in the final solution of 20% glycerol and 0.75 M NaBr for 45 s. MAD data were collected at three wavelengths corresponding to the Br^- peak, inflection, and remote wavelengths calculated by a fluorescence scan on the cryo-cooled crystal at BL 9-2 at SSRL. All native and MAD data sets were processed with DENZO and SCALEPACK (*22*). The MAD data were analyzed by the program SOLVE (*23*) to search for bromide atoms. SOLVE found 13 bromide sites with a figure of merit of 0.29 (0.11 in the highest resolution shell). Solvent flattening was next performed with the program RESOLVE (*24*, *25*), increasing the figure of merit to 0.55.

Model Building and Refinement. Phases taken from RESOLVE were used by the structure building program ARP/wARP (*26*). Phase extension to the high-resolution data set was performed, followed by model building. ARP/wARP built 89% of the residues in the asymmetric unit over the course of 100 cycles. Further model building was carried out with the molecular graphics program ***O*** (*27*). Energy minimization and *B*-factor refinement were carried out with the program CNS (*28*) using 95% of the data to 1.43 Å. During each stage of refinement, the *R*-free and *R*-factor decreased. Noncrystallographic restraints were not used during refinement, resulting in a lower *R*-free. Refinement was completed, giving a final *R*-factor of 18.0% and a *R*-free of 20.5%. The program PROCHECK (*29*, *30*) determined that 99.6% of the residues fall in the most favorable region and allowed region, and 0.4% of the residues fall in the generously allowed region of a Ramachandran plot.

Ligand Soak. Crystals of the ternary E·ADP·APS complex were placed into a synthetic mother liquor of ammonium sulfate, supplemented with 3 mM ADP and 50 mM $MgCl_2$, but with no APS. Crystals were allowed to equilibrate for up to one week, followed by cryo-cooling and data collection as described previously. Unit cell parameters changed to $a = 83.0$ Å, $b = 83.6$ Å, and $c = 138.3$ Å. A data set to 2.00 Å resolution was collected at BL 9-2 at SSRL. This structure was determined by the molecular replacement method using the program AMoRe (*31*). The search model used was the dimer from the ternary structure with both ligands removed.

RESULTS

Overall Ternary Complex Structure. Despite the low figure-of-merit calculated by SOLVE (0.29), secondary structure was evident in the calculated electron density map. Especially evident were areas of little or no density, corresponding to regions of solvent surrounded by areas of high protein electron density. RESOLVE further increased the clarity of the map. The locations of the ligands were plainly evident because of the high number of electrons in the phosphosulfate and pyrophosphate moieties of APS and ADP, respectively. ARP/wARP was used to build the initial model. Phases from RESOLVE were taken, and phase extension was performed to a native data set at 1.43 Å with ARPw/ARP before automated model building. Overall, 100 rounds of refinement and 10 rounds of model building resulted in 699 residues built and docked to the sequence. The average *B*-factor of the final model is 18.0 $Å^2$, compared to the Wilson *B*-factor plot of 14.8 $Å^2$ for the native data. The final *R*-factor and *R*-free are 18.0% and 20.5%, respectively. The crystallographic statistics are summarized in Table 1.

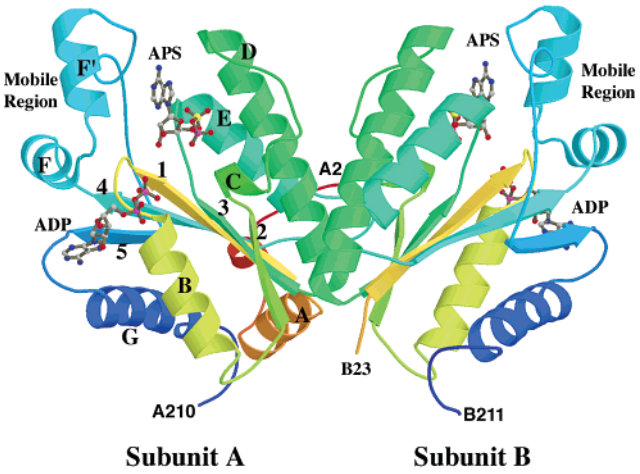

FIGURE 1: Structure of *P. chrysogenum* APS kinase dimer with ligands ADP and APS bound. The ribbon representation is rainbow-colored, with the N-terminus colored in red, ending with blue at the C-terminus for each subunit. The enzyme monomer consists of a five-stranded parallel β-sheet and eight α-helices. The numbering of strands and helices are the same as described previously (*18*), with the addition of helix αF′. The mobile lid region consists of 25 amino acids that form two short helices (F and F′), beginning with residue 145 and ending at 170. The final model consists of residues 2−211 in the A and C subunits, and residues 23−124 and 129−211 in the B and D subunits. ADP binds at the expected P-loop-containing motif. APS binds in a site that lies above ADP in this orientation. The previously disordered region forms approximately half of the binding site for APS. Figures 1, 2A,B, 3B, 4, 5, and 6 were generated using the program MOLSCRIPT (*39*) and rendered with Raster3D (*40*).

The structure of each monomer consists of an open five-stranded parallel β-sheet core between two α-helical bundles (Figure 1). The mobile lid that was previously disordered in the ligand-free structure is observed in this structure and consists of two short α-helices, labeled F and F′. Compared to the ligand-free structure, the overall dimer interface was not changed. There are two dimers present in the crystallographic asymmetric unit: subunits A and B make up one dimer, and subunits C and D make up the other. In monomer A, residues 2−209 (out of 211) were modeled into well-defined electron density, while in monomer B, residues were built from 23 to 122 and from 130 to 211. Monomers C and D follow a similar pattern: subunit C was modeled from 2 to 210 and D from 23 to 124 and from 129 to 209. Thus, monomers A and C are equivalent, and B and D are equivalent. Disordered regions of monomers B and D (residues 125−128) form a loop between αE and β4 and have high *B*-factors in monomers A and C. This loop also had weak density and high-temperature factors in the ligand-free structure (*18*). Sequence alignment of this region reveals

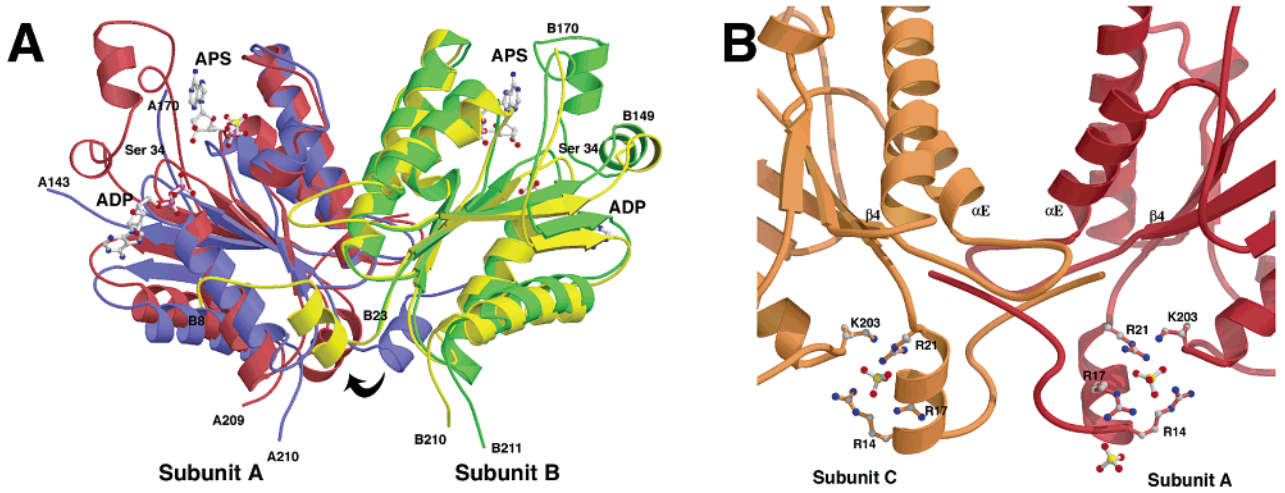

FIGURE 2: (A) Overlay of ternary E·ADP·APS structure (shown in blue and yellow) with the apo enzyme structure (shown in red and green) (PDB 1D6J). The two structures were overlayed along residues 84−98 in helix D from each subunit, which is the major helix running along the dimer interface between monomers. The RMSD for the overlayed residues is 0.322 Å. This figure illustrates the general shift in conformation between the two structures. There is an overall twisting motion of the quaternary structure. This twisting becomes most evident at points of the molecule farthest away from the dimer 2-fold axis. The twisting results in an angle between residue 34 of 5.49° in monomer A and 6.06° in monomer B, calculated from the center of mass at the dimer interface. The black arrow shows the shift in the amino terminus and helix A between the apo structure and the ternary complex structure. (B) N-Terminal interactions that occur among monomers A and C in the ternary complex. Subunit A is colored red, and rotated approximately 90° clockwise along the vertical from A, subunit C is colored orange. The N-terminus is ordered from residue 2 in both of these monomers, but equivalent monomers B and D are ordered beginning with residue 23. Residues 2−22 wind around each other and have three sulfates that are tightly bound to helix A.

that this loop is shorter in the enzymes from nonfungal organisms. Overall, the RMSD of equivalent α-carbon atoms between the A−B dimer compared to the C−D dimer is 0.256 Å for 384 equivalent residues.

In the early stages of crystal screening, vanadate was used to mimic the trigonal bipyramidal transition state of phosphoryl transfer (*32*−*35*). Our hope was to trap a transition-state analogue between the β-phosphate of ADP and the 3′-OH of APS. However, structure determination revealed that vanadate did not bind in the expected active-site position. Instead, vanadate in subunits A and C was coordinated to the 2′-OH and 3′-OH (1.94 and 1.98 Å, respectively) of the ribose ring of ADP. The vanadium also contains two oxygen ligands with distances of 1.73 and 1.49 Å. The fifth ligand is to the 3′-OH (1.90 Å) of a crystal 2-fold symmetry-related ADP bound in the C subunit. Thus, there are two vanadiums (and two ADPs) situated next to the crystal 2-fold axis, with each vanadium being pentavalently coordinated in a quasi-trigonal bipyramidal symmetry. This positioning of vanadate adjacent to the ribose has also been seen in the transition-state structure of ribonuclease A (*36*). Vanadate was not required for crystal growth, but omission from crystallization conditions resulted in lower resolution diffraction (1.65 Å at SSRL; data not shown). Apparently, the vanadium is involved in lattice contacts, which help to stabilize the crystal, but the ion does not form any contacts with the protein and does not bind to the β-phosphate of ADP.

The amino terminus and helix αA shift dramatically compared to the equivalent regions in the ligand-free structure (Figure 2A). In the latter, the N-terminus, beginning with residue 8, and helix αA make significant inter-subunit contacts across the dimer. In the E·ADP·APS structure, the N-terminal residues and helix αA in subunits A and C are shifted away from the opposite monomer and form new contacts (Figure 2B). Helix αA makes more intra-subunit contacts, while the N-terminus is clamped between the αE−β4 loop and the N-terminus of a symmetry-related C-subunit (which is itself shifted like the A subunit). This αE−β4 loop consists of the disordered residues in the B and D monomers and is not conserved among all APS kinases. In the equivalent B and D subunits, the N-terminus and helix αA are completely disordered, with residue 23 being the first residue that can be seen.

Within each A and C monomer, a sulfate ion mediates intra-subunit interactions between residues of αG and the newly shifted helix αA (Figure 2B). The guanido group of arginine residues 14, 17, and 21 of helix αA hydrogen-bond to an ordered sulfate, along with Lys 203 located in helix αG near the C-terminus. Another sulfate ion forms an N-terminal helix cap of helix αA and hydrogen-bonds to main-chain N of Arg 14 at the start of helix αA. This αA helix cap is only observed in the A subunit. These sulfate interactions appear to help hold the N-terminus in this new conformation in subunits A and C. Electron density maps calculated from data collected on crystals not transferred into ammonium sulfate revealed that the N-terminus and helix αA are disordered in subunits A and C (as they are in subunits B and D). This helps explains the significant increase in diffraction upon transfer into ammonium sulfate.

The shifting of the N-terminus and helix αA away from the inter-subunit contacts observed in the ligand-free structure may be functionally relevant because these residues swing back to the original ligand-free position in the binary E·ADP structure formed upon soaking out APS (see below). The interactions of the N-terminus with the sulfates and symmetry-related subunits likely secure the N-terminus into the ordered state seen in the crystal.

Compared to the structure of the apo enzyme reported earlier, the core of the E·ADP·APS structure has changed relatively little (Figure 2A). Alignment of the two αD helices at the dimer interface between both structures (residues 84−98, RMSD 0.322 Å) shows that the dimer interface has not

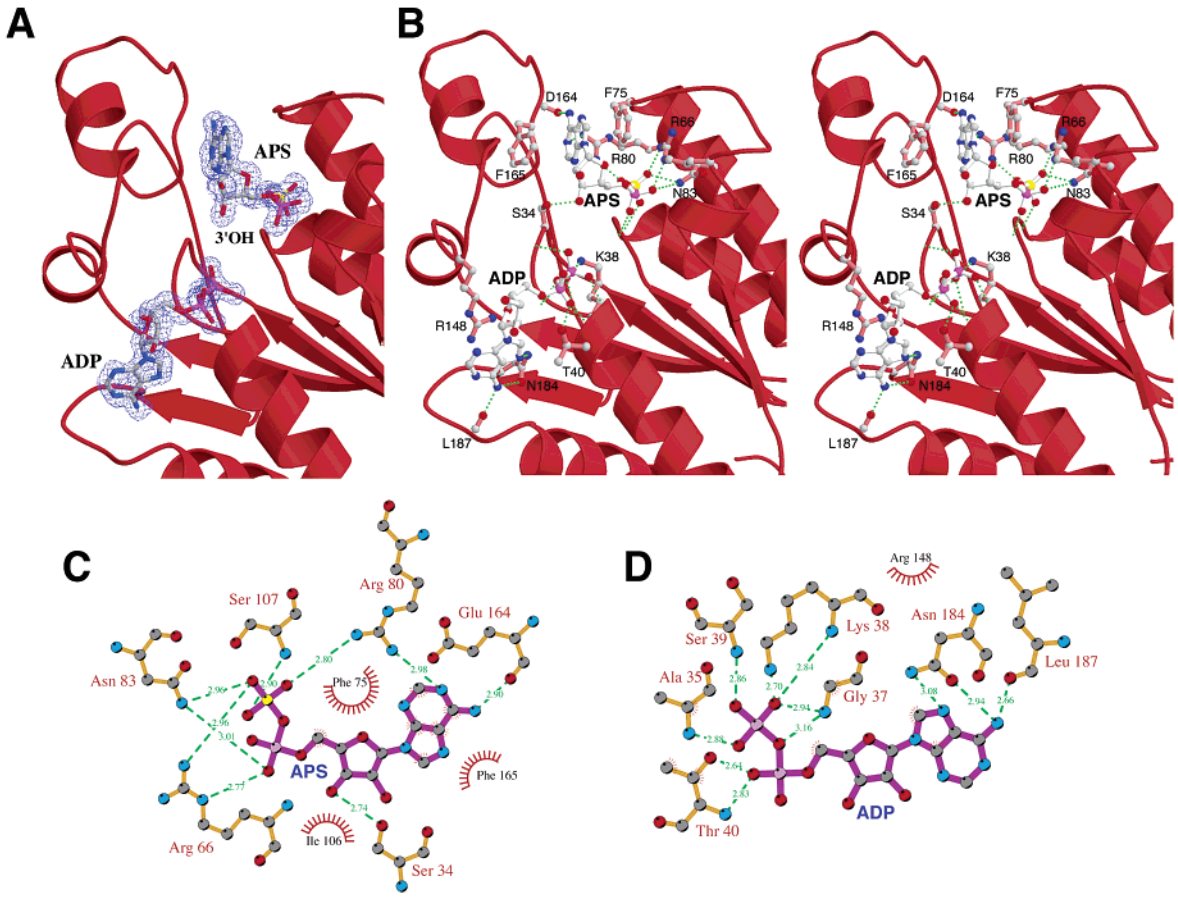

FIGURE 3: Ligand binding sites. (A) Final electron density map calculated with phases from the final model. In blue is a 1.43 Å resolution $|F_o| - |F_c|$ simulated annealing omit map drawn at 3.0σ, calculated by omitting ADP and APS. This figure was generated using the program BOBSCRIPT (*41*). (B) Stereoview of the active site, showing ligands and residues involved in binding. Hydrogen bonds are shown in green dashed lines. (C, D) Flattened image showing protein and ligand interactions for APS and ADP, respectively. Covalent bonds are drawn in purple for ligands and protein bonds in orange. Hydrogen bonds are drawn as green dashed lines with corresponding distances. Van der Waals contacts are drawn with hashed lines between the appropriate atoms on the ligands and residues or atoms of the protein. Figure calculated by LIGPLOT (*42*).

changed. However, at distances farther away, the structural differences can best be described as a general twisting of the subunits with respect to each other. This is evident when comparing the overall shift in the P-loop residues. The Cα of Ser 34, which is close to the 3′-OH that is phosphorylated, shifts by 2.40 Å in subunit A and 2.59 Å in subunit B. This overall twisting results in a rotation in the subunits of 5.49° for subunit A and 6.06° for subunit B (based on the center of mass at the dimer interface and the shift in Ser 34 positions). The net result is a "closing" of enzyme when substrates are bound.

Ligand Binding. The APS kinase reaction follows a sequential ordered mechanism in which MgATP binds before APS, and PAPS leaves prior to MgADP (*6*, *16*). Because of the ordered mechanism, a dead-end E·ADP·APS complex forms readily. (APS adds to the subsite left vacant after PAPS leaves.) It was shown previously that the addition of MgADP and APS protected the enzyme from trypsin cleavage at Arg 158. This trypsin-sensitive site is located in the disordered mobile lid in the ligand-free crystal structure (*18*). The mobile lid was proposed to act as a lid, which closed over the active site when substrates are bound.

In the structure shown in Figure 3A, both ADP and APS are bound at all four active sites in the asymmetric unit. As expected, ADP is present at the P-loop binding site. Arg 148 interacts with the adenine ring at 3.6 Å in what appears to be π-stacking. Arg 148 is the only residue from the mobile lid that makes contact with ADP. In the ligand-free structure, residue 148 was only modeled for subunit B as an alanine; no density was observed for the arginine side chain. It appears that the binding of ADP facilitates the positioning of the mobile lid with the help of Arg 148. The result is a complete binding site for APS. Other residues that interact with the adenine ring of ADP include Asn184 and Leu187. While the ribose ring of ADP does not interact with any part of the protein, the pyrophosphate moiety does so through hydrogen bonds to Ala 35, Gly 37, Lys 38, Ser 39, and Thr 40 (Figure 3B,D). APS is bound above the ADP site. The ribose of APS is in a 3′-endo conformation, with the adenine ring in a syn position above the ribose ring. The adenine ring of APS is sandwiched between Phe 75 (3.58 Å) and Phe 165 (3.48 Å) in a π-stacking arrangement. The 3′-OH, which is phosphorylated during catalysis, hydrogen-bonds with Ser 34 Oγ (2.73 Å) located at the apex of the P-loop. Arg 66, Arg 80, Asn 83, and peptide backbone nitrogens mediate interactions that bind the phosphosulfate moiety (Figure 3B,C). The guanido group of the strictly conserved Arg 66 hydrogen-bonds to sulfate and phosphate oxygen atoms of APS, as do peptide backbone nitrogens of residues Ile 106 and Ser 107. Arg 80, which is another conserved

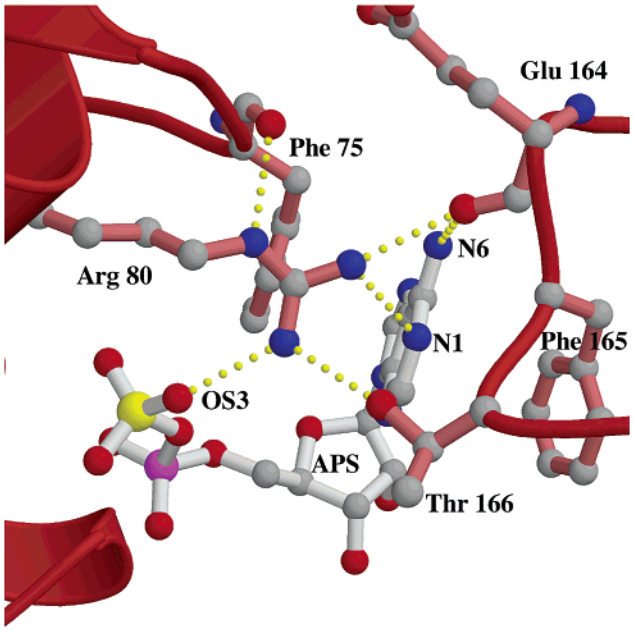

FIGURE 4: Key interactions that arginine 80 plays in forming the active site and binding APS. Strictly conserved Arg 80 forms hydrogen bonds with the substrate at N1 in the adenine ring and OS3 of the phosphosulfate moiety. So, in essence, Arg 80 tethers both ends of the APS molecule. Arg 80 additionally hydrogen-bonds to two points in the APS binding motif of the mobile lid: to Oγ1 of Thr 166 residue and the carbonyl oxygen of Glu 164. Along with this, the Nϵ of Arg 80 bonds to the carbonyl oxygen of Phe 75, which helps orientate it to form the π-stacking interaction with the adenine ring of APS.

residue, makes several key contacts that are crucial to APS binding. Nitrogen Nη2 hydrogen-bonds to N1 of the adenine ring of APS as well as the carbonyl oxygen of Glu 164. Nitrogen Nη1 hydrogen-bonds to a sulfate oxygen in the phosphosulfate moiety of APS and to Thr 166 Oγ1 (Figure 4). Thus, both terminal nitrogens of Arg 80 hydrogen-bond to APS and to the "lid", thereby orientating the substrate and the binding site for subsequent catalysis. Also, the Nϵ of Arg 80 interacts with the carbonyl oxygen of Phe 75, which π-stacks with APS. Overall, Arg 80 forms five important hydrogen-bonding interactions in the binding site of APS. Nδ2 of Asn 83 hydrogen-bonds with both sulfate and phosphate oxygen atoms of the phosphosulfate group. This residue is almost completely conserved. (It is replaced by histidine in two known sequences.)

APS kinase from *E. coli* has been reported to transfer the phosphoryl group by way of a phosphorylated enzyme intermediate at Ser 109 (analogous to Ser 107 in the fungal enzyme) (*10*). In the ternary E·ADP·APS structure of the fungal enzyme, Ser 107 lies below the APS binding site and hydrogen-bonds through its backbone nitrogen to the sulfate of APS. The side-chain oxygen lies 10.6 Å from the β-phosphorus of ADP and is positioned on the wrong side of the protein backbone to participate in phosphoryl transfer. Thus, if this structure is similar to the catalytically active E·MgATP·APS complex, Ser 107 cannot act as a phosphoenzyme intermediate in the fungal enzyme. The structure corroborates mutagenesis experiments showing the nonessentiality of Ser 107 (*17*).

Structure of E·ADP. Crystals grown in the presence of 3 mM APS and 3 mM ADP were moved into a new mother liquor of 1.7 M $(NH_4)_2SO_4$ and 100 mM Bis-Tris Cl (pH 6.5) which contained 3 mM ADP, but no APS. The new mother liquor also contained 50 mM $MgCl_2$, in our hope of determining the binding site for magnesium. A data set was collected at BL 9-2 at SSRL to 2.0 Å (Table 1). To solve the structure, molecular replacement was necessary and was performed with AMoRe using the ternary dimer structure but with both substrates omitted. There are two dimers in the asymmetric unit, and the unit cell dimensions changed to $a = 83.0$ Å, $b = 83.6$ Å, and $c = 138.3$ Å. Overall, there is no observed density for APS in the A and D monomers. There is, however, a sulfate that is bound in the same position as the original phosphate of APS. In the B and C monomers, partial density for APS was observed. Upon modeling in the APS, group-occupancy refinement was carried out by the program CNS to determine an occupancy of 0.55. Density is still discontinuous, but *R*-free was decreased by 0.3% with the addition of this partially occupied APS. This indicates that APS was still bound in some of these subunits, probably because of crystal contacts that hindered diffusion of the ligand.

There are several structural changes that occur as a result of removing APS from the active site (Figure 5A). Examining an overlay between the E·ADP·APS and E·ADP structures reveals that the backbone of the loop between helices αC and αD in the latter shifts by approximately 2.5 Å at Phe 75. (Phe 75 is one of the conserved residues that bind APS.) This shift is in a direction away from the APS binding position. The other half of the binding pocket, formed by the previously disordered region in the apo structure, also shifts away from the position occupied in E·ADP·APS by 1.14 Å at the backbone of Phe 165 (which π-stacks against the adenine ring of bound APS). The overall changes constitute an "opening" of the binding pocket. In the ternary complex, the distance between the α carbons of Phe 75 and Phe 165 is 8.39 Å. In the binary complex, the distance is 11.49 Å.

In the absence of bound APS, the conserved residues Arg 66 and Arg 80 (that normally would interact with APS) are solvent exposed and become more mobile with discontinuous and broken density. Arg 80, which makes several contacts with other protein residues to help define the APS binding pocket when APS is bound, shifts toward the vacant APS binding site and hydrogen-bonds to a solvent molecule in the APS-free structure. This suggests an "induced fit" conformational change upon APS binding, in which Arg 80 supplies additional APS binding energy by interacting with residues in the APS binding pocket as well as with APS.

Another striking conformational difference between E·ADP·APS and E·ADP occurs in the N-terminal region. In E·ADP·APS, residues 2−23 are ordered only in subunits A and C, and the structure of these residues is mediated by crystal contacts and sulfate (see above). In the E·ADP structure, the N-terminal residues are ordered in all four subunits in the asymmetric unit, starting with residue 7. Essentially, the residues have moved back to their original position. As shown in Figure 5B, the positions of these N-terminal residues are nearly identical in the apo enzyme and E·ADP structures. While there is no doubt that the N-termini are highly mobile, the significance of the APS-dependent movement is not yet known.

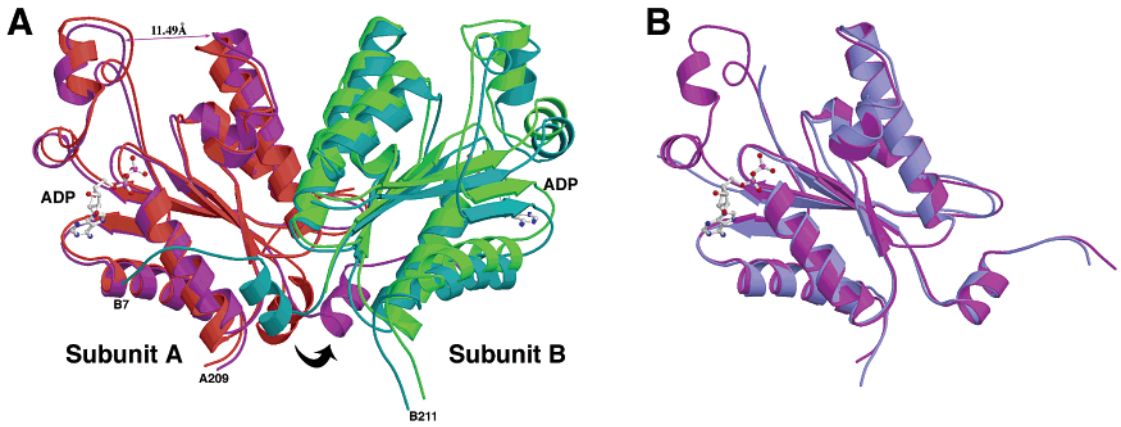

FIGURE 5: (A) Overlay of E·ADP·APS and E·ADP. The two ternary structure monomers are colored red and green. The binary structure monomers are colored purple and dark green. In subunit B, the N-terminal domain is now ordered starting with residue B7. The position is the same as seen in the apo structure. The overlay is based on superposition of the A subunits in each structure. The binding site for APS in the A subunit has "opened", showing the release of the substrate. Overall, the distance between the Cα's of residues 75 and 165 have changed from 8.39 to 11.49 Å. Also evident is the general twisting and opening of the subunits with respect to each other. (B) Overlay of monomers between binary structure and apo structure. The binary structure is shown in purple and the apo in blue. The ADP from the binary structure is shown. After release of APS, the N-terminus and helix αA shift to a nearly identical position, as seen in the apo structure.

DISCUSSION

The structures presented in this report, together with the one reported previously for the apo enzyme, are consistent with a sequence in which MgATP (or MgADP) binds to the P-loop and induces the formation of the APS binding pocket by locking onto Arg 148 of the mobile lid. (Arg 148 is the only residue in the mobile lid that interacts directly with the ADP.) The immobilization of this residue appears to confer enough order to the mobile lid to form the APS binding pocket.

Satischandran et al. (*10*) suggested that the sulfonucleotide binding motif was ^{156}KAREGVIKEFT^{166}. While this sequence is highly conserved among APS kinases, the residues that actually cooperate to bind APS are ^{164}EFT^{166}. Specifically, Thr 166, which is conserved among all species, hydrogen-bonds to Arg 80, which also is completely conserved. Arg 80 interacts directly with APS. Phe 165 is nearly completely conserved across species and π-stacks to the adenine of APS. Other residues that are completely or almost completely conserved include Ala 157, Gly 160, Ile 162, and Gly 167. None of these residues forms direct interactions with APS, but they all probably help to maintain the secondary and tertiary structure essential for forming the binding pocket. Thus, a more general motif for APS binding is ^{157}AXXGXIXXFTG^{167}.

There are three Arg residues in the structure that are completely conserved and form important interactions. Arg 148 of the mobile lid stacks against the adenine ring of ADP. The positioning of this residue upon binding of ADP plausibly positions the remaining residues, which are necessary to form the binding site of APS. The other two key arginine residues, Arg 66 and Arg 80, make extensive interactions with APS and residues that form the APS binding pocket.

Serine 34, which is located in the apex of the P-loop (and is completely conserved among APS kinases), makes a hydrogen bond to the 3′-OH of APS, the group that is phosphorylated by ATP. Ser 34 is the only residue that interacts with the 3′-OH and thus is the only candidate that can serve as a general base for abstracting a proton from the 3′-OH to produce a nucleophile that can attack the γ-phosphorus of ATP. However, there are no neighboring residues near Ser 34 that could help reduce its pK_a, making it a better base at physiological pH. Ser 34 is surrounded only by ordered water molecules. Perhaps Ser 34 plays a different role. For example, *E. coli* APS kinase is believed to proceed via a phosphorylated enzyme intermediate. The phosphoryl acceptor was identified as Ser 109 (*9*), a residue analogous to Ser 107 of the *P. chrysogenum* enzyme. Ser 107 is not essential for activity of the fungal enzyme (*17*), nor can a phosphorylated form of fungal APS kinase be isolated (*8*). Moreover, the reaction kinetics rules out a classical ping-pong mechanism (*6*). Nevertheless, the possibility that a transient phosphoenzyme is indeed an intermediate in the reaction cannot be discarded. In this case, Ser 34 might serve as the phosphoryl acceptor. Experiments are in progress to determine the importance of Ser 34 in catalysis and to determine its pK_a.

Under normal assay conditions (at micromolar levels of APS), Mg^{2+} promotes APS binding and catalysis. However, no Mg^{2+} was observed in the crystal structure, even though Mg^{2+} was included in the crystal setups and subsequent soaks. The close structural relative, 6-phosphofructo-2-kinase/2,6-phosphofructo-2-phosphatase, has been crystallized with ATPγ-S and Mg^{2+}. The Mg^{2+} formed its closest interactions to an oxygen on the γ-phosphate. Possibly, the γ-phosphate of ATP or an analogue is needed in order for Mg^{2+} to bind to APS kinase. It is still unknown if Asp 61 in APS kinase acts as a Walker B motif by coordinating a water which is coordinated to Mg^{2+}.

ATP sulfurylase from *P. chrysogenum*, the first enzyme in the sulfate activation pathway, has an allosteric domain that is analogous to that of APS kinase, sharing 42% identity. This allosteric domain has lost the ability to bind ATP but retains the ability to bind PAPS (*37*) and APS (*38*). The overlay of the allosteric domain of ATP sulfurylase and the monomer of APS kinase (Figure 6) confirms that the tertiary structures are nearly identical. The residues that interact with APS are conserved between the two structures, but the ADP-interacting Arg 148 of APS kinase is not. However, ATP

FIGURE 6: Overlay of APS kinase (E·ADP·APS) and the allosteric domain of *P. chrysogenum* ATP sulfurylase. The ternary complex of APS kinase is shown in red; the allosteric domain is shown in beige. ADP and APS from the ternary complex are shown, but APS bound in the allosteric domain on ATP sulfurylase is virtually identical to APS binding in APS kinase.

sulfurylase is a hexamer in which the mobile lid of the allosteric domain interacts with an inter-subunit catalytic domain. This interaction may help to position the lid for PAPS binding. In APS kinase, there is no quaternary structure to help orient the mobile lid; Arg 148 serves this purpose by interacting with ATP.

At low protein concentrations, fungal APS kinase dissociates completely into inactive monomers (subunits) at $T >$ 42° C. Upon cooling of the heated preparation to 30° C or below, the monomers reassemble, and all of the original activity is regained. The structures described in this report provide a plausible explanation for the inactivity of the monomers: The main secondary structural elements involved in dimer formation are helices αC and αD. The binding site for ATP lies far from the dimer interface, with no apparent relationship to the dimer per se. On the other hand, the APS binding site has a more direct relationship to dimerization. Near the APS binding site at the dimer interface lies a very hydrophilic patch composed of Asp 72, Glu 82, Arg 85, and Arg 86. The majority of interactions of these residues are intra-monomer hydrogen-bonding: Aspartate 72 hydrogen-bonds to Arg 85, which bonds to Glu 82, which bonds to Arg 86. Arg 85 and Arg 86 also participate in inter-subunit interactions. Specifically, the aliphatic portion of the side chain of Arg 86 appears to make van der Waals contact with the 2-fold-related Arg 86 of the other subunit (they lie 3.55 Å apart), while Arg 85 caps the C-terminal carbonyls of Glu 68 and Leu 69 across the interface. These latter residues lie at the end of helix αD. Recall that Arg 66, an important APS binding residue, is located in helix αD (Figure 3B). Thus, the capping may help position and stabilize the helix for binding APS. Several other residues between Asp 72 and Glu 82 in the primary sequence are also important in APS binding. For example, Phe 75 forms one part of the "clamp" that holds APS; Arg 80 holds the APS site together (Figures 3B and 4). Thus, when the subunits separate, a number of interactions that shape the APS binding site are eliminated, even though the site itself is not at the interface. The interaction of the hydrophilic patch with the solvent may help to stabilize the monomer conformation at high temperatures.

Ligand soaks were performed in an attempt to gain more structural information about the sequential ordered mechanism. APS was able to diffuse out freely from one active site and partially from the other active site of the dimer. Overall, structural changes that occurred showed an opening of the binding site by 3.10 Å. More dramatic changes occurred in the N-terminal residues, which shifted from a structure mediated by crystal contacts and bound sulfate molecules to a position that was shown to be preferable in the apo structure. The fact that APS was able to diffuse out of the active site while the mobile lid retained its order suggests that the resulting structure is a plausible intermediate in the catalytic cycle. Earlier studies showed that APS acts as a substrate inhibitor by binding to E·MgADP. This leads to the conclusion that the binding site for APS is structured when ADP is bound.

REFERENCES

1. Lyle, S., Stanczak, J., Ng, K., and Schwartz, N. B. (1994) *Biochemistry 33*, 5920−5925.
2. Venkatachalam, K. V., Akita, H., and Strott, C. A. (1998) *J. Biol. Chem. 273*, 19311−19320.
3. Xu, Z. H., Otterness, D. M., Freimuth, R. R., Carlini, E. J., Wood, T. C., Mitchell, S., Moon, E., Kim, U. J., Xu, J. P., Siciliano, M. J., and Weinshilboum, R. M. (2000) *Biochem. Biophys. Res. Commun. 268*, 437−444.
4. Coughtrie, M. W., Sharp, S., Maxwell, K., and Innes, N. P. (1998) *Chem. Biol. Interact. 109*, 3−27.
5. Franzon, V. L., Gibson, M. A., Hatzinikolas, G., Woollatt, E., Sutherland, G. R., and Cleary, E. G. (1999) *Int. J. Biochem. Cell Biol. 31*, 613−626.
6. Renosto, F., Seubert, P. A., and Segel, I. H. (1984) *J. Biol. Chem. 259*, 2113−2123.
7. Renosto, F., Seubert, P. A., Knudson, P., and Segel, I. H. (1985) *J. Biol. Chem. 260*, 11903−11913.
8. Renosto, F., Martin, R. L., and Segel, I. H. (1991) *Arch. Biochem. Biophys. 284*, 30−34.
9. Satishchandran, C., and Markham, G. D. (1989) *J. Biol. Chem. 264*, 15012−15021.
10. Satishchandran, C., Hickman, Y. N., and Markham, G. D. (1992) *Biochemistry 31*, 11684−11688.
11. Satishchandran, C., and Markham, G. D. (2000) *Arch. Biochem. Biophys. 378*, 210−215.
12. Lee, S., and Leustek, T. (1998) *Biochem. Biophys. Res. Commun. 247*, 171−175.
13. Lillig, C. H., Schiffmann, S., Berndt, C., Berken, A., Tischka, R., and Schwenn, J. D. (2001) *Arch. Biochem. Biophys. 392*, 303−310.
14. Lyle, S., Ozeran, J. D., Stanczak, J., Westley, J., and Schwartz, N. B. (1994) *Biochemistry 33*, 6822−6827.
15. Deyrup, A. T., Krishnan, S., Singh, B., and Schwartz, N. B. (1999) *J. Biol. Chem. 274*, 10751−10757.
16. MacRae, I. J., and Segel, I. H. (1999) *Arch. Biochem. Biophys. 361*, 277−282.
17. MacRae, I. J., Rose, A. B., and Segel, I. H. (1998) *J. Biol. Chem. 273*, 28583−28589.
18. MacRae, I. J., Segel, I. H., and Fisher, A. J. (2000) *Biochemistry 39*, 1613−1621.
19. Walker, J. E., Saraste, M., Runswick, M. J., and Gay, N. J. (1982) *Embo. J. 1*, 945−951.
20. Dauter, Z., and Dauter, M. (1999) *J. Mol. Biol. 289*, 93−101.
21. Dauter, Z., Dauter, M., and Rajashankar, K. R. (2000) *Acta Crystallogr., Sect. D: Biol. Crystallogr. 56* (Pt. 2), 232−237.
22. Otwinowski, Z. M., W. (1997) *Methods in Enzymology*, pp 307−326, Academic Press, New York.
23. Terwilliger, T. C., and Berendzen, J. (1999) *Acta Crystallogr., Sect. D: Biol. Crystallogr. 55* (Pt. 4), 849−861.
24. Terwilliger, T. C. (1999) *Acta Crystallogr., Sect. D: Biol. Crystallogr. 55*, 1863−1871.
25. Terwilliger, T. C. (2000) *Acta Crystallogr., Sect. D: Biol. Crystallogr. 56* (Pt. 8), 965−972.
26. Perrakis, A., Morris, R., and Lamzin, V. S. (1999) *Nat. Struct. Biol. 6*, 458−463.

27. Jones, T. A., Zou, J. Y., Cowan, S. W., and Kjeldgaard, M. (1991) *Acta Crystallogr., Sect. A: Found. Crystallogr. 47*, 110−119.
28. Brunger, A. T., Adams, P. D., Clore, G. M., DeLano, W. L., Gros, P., Grosse-Kunstleve, R. W., Jiang, J. S., Kuszewski, J., Nilges, M., Pannu, N. S., Read, R. J., Rice, L. M., Simonson, T., and Warren, G. L. (1998) *Acta Crystallogr., Sect. D: Biol. Crystallogr. 54* (Pt. 5), 905−921.
29. Ramakrishnan, C., and Ramachandran, G. N. (1965) *Biophys. J. 5*, 909−933.
30. Laskowski, R. A., Macarthur, M. W., Moss, D. S., and Thornton, J. M. (1993) *J. Appl. Crystallogr. 26*, 283−291.
31. Navaza, J. (1993) *Acta Crystallogr., Sect. D: Biol. Crystallogr. 49*, 588−591.
32. Goodno, C. C. (1982) *Methods Enzymol 85* (Pt. B), 116−123.
33. Lindqvist, Y., Schneider, G., and Vihko, P. (1994) *Eur. J. Biochem. 221*, 139−142.
34. Smith, C. A., and Rayment, I. (1996) *Biochemistry 35*, 5404−5417.
35. Zhang, M., Zhou, M., VanEtten, R. L., and Stauffacher, C. V. (1997) *Biochemistry 36*, 15−23.
36. Ladner, J. E., Wladkowski, B. D., Svensson, L. A., Sjolin, L., and Gilliland, G. L. (1997) *Acta Crystallogr., Sect. D: Biol. Crystallogr. 53*, 290−301.
37. MacRae, I., and Segel, I. H. (1997) *Arch. Biochem. Biophys. 337*, 17−26.
38. MacRae, I. J., Segel, I. H., and Fisher, A. J. (2001) *Biochemistry 40*, 6795−6804.
39. Kraulis, P. J. (1991) *J. Appl. Crystallogr. 24*, 946−950.
40. Merritt, E. A., and Murphy, M. E. P. (1994) *Acta Crystallogr., Sect. D: Biol. Crystallogr. 50*, 869−873.
41. Esnouf, R. M. (1997) *J. Mol. Graph. Model. 15*, 132−134; 112−113.
42. Wallace, A. C., Laskowski, R. A., and Thornton, J. M. (1995) *Protein Eng. 8*, 127−134.

BI026556B